A Computationally Efficient 2D-root MUSIC Parameter Estimation for OCDM-based RadCom

Amna Javed Tiwana[1], Paul Townsend[1], Holger Claussen[1,2], and Xing Ouyang[1]

[1,2] Tyndall National Institute, University College Cork, Ireland
[2]Trinity College Dublin, Ireland
[1,2]{amna.tiwana|paul.townsend|holger.claussen|xing.ouyang}@tyndall.ie

***Abstract*—The next-generation of wireless communication is anticipated to integrate sensing and communication using a unified yet versatile waveform, capable of providing not only reliable data communication, but also localization and sensing functionality. Given the chirp-based structure of the recently proposed orthogonal chirp division multiplexing (OCDM), it has shown robustness against frequency selectiveness for communication but also suitability for sensing because of the inherent pulse compression property of the chirps. Although OCDM-based spectral resolution algorithms have been explored, polynomial root-based multiple signal classification (MUSIC) poses the issues of high-dimensionality and correct estimation assignment, especially for highly correlated multiple targets. In this paper, a computationally efficient two-dimensional high-resolution algorithm is proposed for joint range-velocity estimation for the OCDM-based Radar-Communication (RadCom) system. The proposed frequency domain radar processing for OCDM utilizes the eigen-decomposition property of the Fresnel transform through a reduced polynomial-based root MUSIC algorithm, in conjunction with Gaussian pulses, to jointly localize synchronized targets. Polynomial dimensionality has been reduced by transforming the nonlinear polynomial into a linear eigenvalue problem. The eigen structure of the signal subspace is utilized to resolve the issue of estimation assignment for highly correlated multiple targets by minimizing the residual projection error. The numerical results for the proposed chirp-based pilot sensing demonstrate a significant improvement in sidelobes reduction over the typical 2D-FFT and 2D-MUSIC approach, for uncorrelated and highly correlated targets. Moreover, the algorithm avoids 2D exhaustive search as in conventional 2D-MUSIC, meanwhile, reducing the computational overhead of traditional OCDM radar processing.**

***Index Terms*—OCDM RadCom, 2D root-MUSIC, Correlated signals**

I. Introduction

The integration of radar detection and communication (RadCom), often referred to as joint communication and sensing (JCAS) or integrated sensing and communication (ISAC), has been gaining major traction for next-generation standards. The use of a single communication waveform could enhance system flexibility and energy efficiency, meanwhile, paving the way for cost effectiveness and reduction of the device footprint as well [1], [2]. The optimization parameters for radar systems are high-resolution target detection in terms of range, direction-of-arrival (DoA), and velocity, whereas, low latency, high reliability, and high data rates are desirable for a communication waveform.

A significant development for orthogonal frequency division multiplexing (OFDM) radar was proposed in [3], by incorporating modulated symbols for radar processing rather than the baseband signal, thus completely eliminating user data from the sensing algorithm. Given the compatibility with OFDM, several digital multicarrier modulation schemes have been explored [4], such as orthogonal time frequency space (OTFS) [5], affine frequency division multiplexing (AFDM) [6], and OCDM [7], to overcome the shortcomings of OFDM for communication and/or sensing.

Due to robustness against frequency selective fading and better spectral efficiency, a discrete Fresnel transform (DFnT) based OCDM was proposed as a counterpart to traditional OFDM for wireless communication [8]. An OCDM-based RadCom system was proposed in [7], whereby Discrete Fourier Transform (DFT) processing is applied before radar image processing based on the 2D-FFT approach on the traditional time-domain OCDM waveform. However, the proposed methodology results in higher computational complexity as well as sidelobes. A sequential symbol decoding and radar parameter estimation (SUNDAE) algorithm based on OCDM with 2D-FFT/periodogram-based detection was proposed in [9]. In [10], a multistage sensing algorithm was proposed using an optimal weighted combiner from different sensing processors, which puts a strain on computational complexity.

Along with that, the typical 2D-FFT approach employed for multicarrier schemes is restricted by the inherent Rayleigh resolution limit of the radar. Thus, subspace-based super-resolution algorithms, such as multiple signal classification (MUSIC) [11] and estimation of signal parameters via rotational invariance techniques (ESPRIT) [12], were introduced for estimation beyond the inherent limit of the radar. Although these algorithms were introduced mainly for the direction-of-arrival (DoA) estimation, the algorithms could be easily extrapolated for the range-velocity estimation as well [3], [13].

In the present study, we investigate the frequency domain processing of OCDM using the eigen decomposition property of the Fresnel transform, which minimizes the computational complexity by eliminating additional DFT processing on the conventional time domain OCDM symbols. We propose a 2D-root MUSIC algorithm, while reducing polynomial dimensionality by transforming non-linear root-finding polynomial into linear eigenvalue problem and resolving the estimation

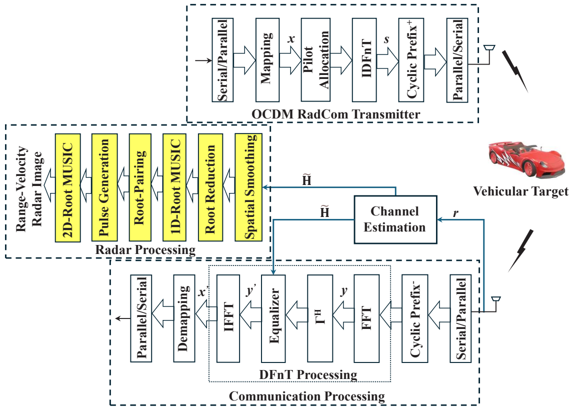

Fig. 1. Block representation of OCDM RadCom system

assignment issue of classical root MUSIC using the signal subspace structure, in conjunction with Gaussian pulses to obtain the target estimation. The proposed methodology avoids the 2D exhaustive search as in the 2D-MUSIC approach, and estimates synchronized range-velocity pairs.

The remainder of the article is organized with a brief description of the system model for communication processing in Section II. The formulation of the radar processing problem is explained in Section III, while the proposed algorithm is elaborated in Section IV. The simulated results for uncorrelated and correlated targets are discussed in Section V, and finally Section VI concludes the paper.

II. Communication Processing

A. OCDM Transmitted Signal

The discrete-time OCDM signal can be represented in matrix form as

$$\mathbf{s} = \mathbf{\Phi}^H \boldsymbol{x}, \tag{1}$$

where the vector $\boldsymbol{x}$ is the stacked input symbols for an OCDM block with N orthogonal chirps of size $N \times 1$, and the DFnT basis matrix of size $N \times N$ is given as

$$\Phi(m,n) = \frac{1}{\sqrt{N}} e^{-j\frac{\pi}{4}} \times \begin{cases} e^{j\frac{\pi}{N}(m-n)^2}, & N \equiv 0 (mod2) \\ e^{j\frac{\pi}{N}(m+\frac{1}{2}-n)^2}, & N \equiv 1 (mod2). \end{cases} \tag{2}$$

Chirp-based channel estimation is performed, where a family of orthogonal chirps is used, so that the reference symbols are still separable after pulse compression (matched filtering with DFnT) at the receiving end [14]. The system diagram is shown in Fig. 1.

B. OCDM Received Signal

Considering the presence of L target reflections, the range r_l of the target l, where $l = 0, 1, ..., L-1$, is depicted by the delay τ_l suffered by the reflected signal is given as $\tau_l = \frac{2\times r_l}{c}$. Similarly, the Doppler shift f_{D_l} caused by the relative velocity v_l between the target and the radar is given by $f_{D_l} = \frac{2\times f_c \times v_l}{c}$, where f_c is the carrier frequency of the transmitter and c is the speed of light. The received OCDM signal after passing through the channel $\boldsymbol{h}$, while ignoring the additive Gaussian noise, can be given as

$$\mathbf{r} = \mathbf{h} \circledast \mathbf{s}. \tag{3}$$

Here, $\circledast$ is the circular convolution operator resulting from the cyclic prefix, which converts linear convolution to circular convolution. The doubly dispersive channel for l-th scatterer with h_l path gain, can be represented as

$$h(n,l) = \sum_{l=0}^{L-1} h_l \delta(\frac{nT}{N} - \tau_l) e^{j2\pi f_{D_l}(\frac{nT}{N}-\tau_l)}, \tag{4}$$

where T is the OCDM symbol period and δ is the delayed channel response. Thus (3) becomes

$$\begin{aligned} r(n,l) &= \sum_{l=0}^{L-1} h_l s(\frac{nT}{N} - \tau_l) e^{j2\pi f_{D_l}(\frac{nT}{N}-\tau_l)} \\ &= \frac{1}{\sqrt{N}} e^{j\frac{\pi}{4}} \sum_{l=0}^{L-1}\sum_{n=0}^{N-1} h_l x(\frac{nT}{N} - \tau_l) e^{j2\pi \frac{f_{D_l}}{N}(nT - \tau_l \frac{N}{T})} \\ &e^{j\frac{\pi}{N}\{(m-n)-\tau_l \frac{N}{T}\}^2}. \end{aligned} \tag{5}$$

The received OCDM signal is then matched filtered using DFnT, using the eigen decomposition of DFnT to perform the single-tap frequency domain equalization in order to recover the communication data symbol as in [8], [14].

III. Radar Signal Processing

A. Radar Processing Channel Matrix

Given the circulant nature and convolution preservation property of the discrete Fresnel transform, the eigen-decomposition of DFnT into frequency domain symbols using DFT allows us to obtain the channel frequency response (CFR) directly [8]. The frequency domain received reference symbols after DFT operation ($\mathbf{F}$) are given as

$$\mathbf{y} = \mathbf{F}\mathbf{H}\mathbf{\Phi}^H \boldsymbol{x}, \tag{6}$$

where

$$y(m,l) = \Gamma^H(m) \sum_{l=1}^{L} H(m,l) \mathbf{F}\{r(n-\tau_l)\}. \tag{7}$$

Here, $H(m,l) \coloneqq \mathbf{F}\{h(n,l)(m)\}$ and $\Gamma^H(m)$ is the phase coefficient or essentially the eigen values of IDFnT w.r.t DFT [15]. Unlike conventional digital pulse compression via Hadamard product with the complex conjugate of the resulting matrix from the DFT-transformed copy of transmit symbols [7], the phase-compensated CFR in (7) is utilized for radar processing. Thus, the adaptability of DFnT to FFT and IFFT eliminates the need for additional computational overhead in terms of Hadamard product and DFT blocks.

B. Problem Formulation

The most common way for target estimation is the 2D-FFT or periodogram method, where IFFT is taken across the subcarriers and FFT across time axis of the radar processing matrix [3], to estimate range and velocity, respectively. However, the resolution of this method is restricted by the rayleigh limit of the radar, with a range resolution of $\Delta r = \frac{c}{2N\Delta f}$ and a velocity resolution of $\Delta v = \frac{c}{2MT_0 f_c}$, where Δf is the subcarrier spacing and T_0 is the total symbol period along with the cyclic prefix.

Some spectrally efficient subspace-based super-resolution algorithms, such as MUSIC and ESPRIT, originally proposed for the direction-of-arrival (DoA) estimation, could be utilized to improve the range and velocity resolution as well. 1D-MUSIC algorithm utilizes the Doppler exponential across the OCDM symbols as a steering vector for velocity estimation, while the delay exponential across the subcarriers acts as a steering vector for range detection [11]. The principle of this method lies in the assumption that the noise subspace is orthogonal to the steering vector at a particular value of range (velocity), and is obtained by the following pseudospectrum in (8). However, being a single-dimensional algorithm when the number of targets is more than one, it is not possible to associate range and velocity peaks correctly.

$$P_{MUSIC} = \frac{1}{\boldsymbol{v(\psi)}^H \boldsymbol{E_N} \boldsymbol{E_N}^H \boldsymbol{v(\psi)}}. \tag{8}$$

Here, $\boldsymbol{E_N}$ is the noise subspace matrix and $\boldsymbol{v(\psi)}$ is the steering vector, which depending on the estimation, could be the range $\boldsymbol{v_r}$ or Doppler $\boldsymbol{v_d}$ steering vectors as follows

$$\boldsymbol{v_r} := e^{-j2\pi n \Delta f \tau_l}, \qquad \text{when} \quad n = 0, 1, ..., N-1, \tag{9}$$
$$\boldsymbol{v_d} := e^{j2\pi m f_{D_l} T_0}, \qquad \text{when} \quad m = 0, 1, ..., M-1. \tag{10}$$

MUSIC for the joint estimation of range and velocity is obtained by combining the steering vectors for range and velocity by vectorization [16]. Thus, in this case, the steering vector becomes a combination of both vectors using a Kronecker Product ($\otimes$)

$$\boldsymbol{v(\psi)} = \boldsymbol{v_r} \otimes \boldsymbol{v_d} \in \mathbb{C}^{(NM)\times 1}. \tag{11}$$

Since the method incorporates only a single snapshot of the OCDM symbol due to the vectorization operation, spatial smoothing is required to compensate for the correlation of incoming signals. Moreover, smoothing also helps reduce dimensionality by reducing the off-diagonal elements of the covariance matrix by averaging the sub-arrays [16], [17].

Unlike peak search using the pseudospectrum, Root-MUSIC allows us to directly calculate the roots of the polynomial used in the denominator of (8). In the absence of noise, the polynomial roots present on the unit circle would correspond to the steering vectors that are completely orthogonal to the noise subspace; however, due to the presence of noise, we consider L roots inside and closest to the unit circle. These roots allow us first to estimate the respective delays and Doppler associated with each target, and eventually the range and velocity in the following manner

$$\hat{\tau}_l = -\frac{\theta_{R_{range}}}{2\pi\Delta f}, \tag{12}$$

$$\hat{r}_l = \frac{\hat{\tau}_l c}{2}, \tag{13}$$

$$\hat{f}_{D_l} = \frac{\theta_{R_{vel}}}{2\pi T_0}, \tag{14}$$

$$\hat{v}_l = \frac{\hat{f}_{D_l} c}{2 f_c}. \tag{15}$$

Here, $\theta_{R_{range}}$ and $\theta_{R_{vel}}$ are angles of the roots of the range and velocity covariance matrices, respectively.

Although the MUSIC algorithm provides us with a defined spectral peak, it becomes an exhaustive search especially in multi-target detection, i.e, 2D-MUSIC. The issue of extensive root-finding for the double polynomial also needs to be mitigated. Moreover, the issue of root-pair assignment for multiple correlated targets also requires attention, since the pulses have to be generated based on the correct assignment of range-velocity pair to each target. Thus, in order to avoid the computationally inefficient spectral search for 2D-MUSIC psudeospectrum, in the present work we are interested in utilizing the 1D-root MUSIC estimates, via reduced-degree polynomial, to develop a simplified 2D-root MUSIC algorithm for synchronized estimation.

IV. Proposed method

The complexity of searching the entire range and velocity steering vectors for joint parameter estimation in the presence of multiple targets requires simplified ways to improve spectral resolution. To solve this problem, we propose the utilization of the 1D-root MUSIC algorithm in conjunction with specifically designed Gaussian pulses, to achieve the 2D-root MUSIC estimates, as depicted in Fig. 1. Since the roots of the pseudospectrum function appear as conjugate pairs, which for a double polynomial (in our case, two single polynomials) results in finding a sum of $2 \times (N_s - 1)$ and $2 \times (M_s - 1)$ roots, where N_s and M_s are the subcarriers and symbols after smoothing, respectively. To further reduce the computational complexity of such extensive root-finding, we incorporate the shift-inversion method to make the eigenvalues closest to the unit circle the most dominant and then utilize the Krylov-Schur algorithm [18] to attain only those eigenvalues. Let the N-th degree root-finding polynomial $q(z)$, with coefficients $c_0, c_1, ..., c_{N-1}$ from the psuedospectrum function (8) is given as

$$q(z) = z^N + c_{N-1} z^{N-1} + ... + c_1 z + c_0. \tag{16}$$

To convert the non-linear root finding into linear eigenvalue problem, the squared companion matrix $\boldsymbol{Q}$ of size $N \times N$ is formulated, the first row of which is given by the polynomial coefficients and the sub-diagonal elements set to 1 as

$$\boldsymbol{Q} = \begin{bmatrix} -c_{N-1} & -c_{N-2} & \cdots & -c_1 & -c_0 \\ 1 & 0 & \cdots & 0 & 0 \\ 0 & 1 & \cdots & 0 & 0 \\ \vdots & & \ddots & \vdots & \\ 0 & 0 & \cdots & 1 & 0 \end{bmatrix}. \tag{17}$$

Since the eigenvalues of the matrix thus formulated are the roots of the original polynomial, using the shift-invert transform would make the eigenvalues nearest to the unit-circle larger in magnitude as follows

$$\boldsymbol{R} = \frac{1}{\boldsymbol{Q} - (e^{j\frac{\pi}{4}})\boldsymbol{I}}, \tag{18}$$

where $\boldsymbol{I}$ is the identity matrix of size $N \times N$, and the exponential represents the threshold, that is, the unit circle. Thus, we can now obtain the highest eigenvalues, in other words, the roots of a much lower-degree polynomial. In our analysis, we have selected the first $N_s - 1$ and $M_s - 1$ highest eigenvalues, thus reducing the polynomial roots to half.

Before the formulation of Gaussian pulses, the assignment of correct range-velocity pairs needs to be done for multiple highly correlated targets. Using the signal subspace structure, we have incorporated Hungarian algorithm, also known as the Kuhn-Munkres algorithm [19], to find the optimal assignment of ranges to velocities so that the projection residual error is minimized. Once the target estimates from 1D-root MUSIC are obtained, we construct a 2D-steering vector of size $N_s M_s \times 1$, based on the range and velocity steering vectors for all estimated values as in (10). The signal subspace $\boldsymbol{E_s}$ of size $N_s M_s \times L$ is obtained from the spatially smoothed 2D covariance matrix. The residual projection cost function is then given by the Euclidean norm as

$$\boldsymbol{E_p} = ||(\boldsymbol{I} - \boldsymbol{E_s}\boldsymbol{E_s}^H)\boldsymbol{v}(\boldsymbol{\psi})||^2. \tag{19}$$

Here, the projection error matrix $\boldsymbol{E_p}$ of size $L \times L$ contains the residual norm between each pair of range-velocity and the signal subspace, and $\boldsymbol{I}$ is the identity of size $N_s M_s \times N_s M_s$. Once the cost function is obtained, the linear assignment problem can be solved for each row and column such that each row is assigned to a column in a way that the total cost is minimized. This operation allows us to assign the right pairs of range-velocity, since only the right pair would provide the maximum correlation with the signal subspace and thus the minimum $\boldsymbol{E_p}$.

The utilization of pulses allows flexibility to control the sidelobes and that helps in target separation when they are highly correlated. More precisely, the single dimension estimates from the root-MUSIC algorithm in (13) and (15) are used to compute the following pulses with peaks set at the estimated values as

$$\begin{aligned}\boldsymbol{\delta_{\hat{r}_l}} &= e^{-\frac{(t_r - \hat{r}_l)^2}{2\sigma^2}}, \\ &= e^{-\frac{(t_r - (\frac{\hat{\tau}_l c}{2}))^2}{2\sigma^2}} + eps,\end{aligned} \tag{20}$$

$$\begin{aligned}\boldsymbol{\delta_{\hat{v}_l}} &= e^{-\frac{(t_v - \hat{v}_l)^2}{2\sigma^2}}, \\ &= e^{-\frac{(t_v - (\frac{\hat{f}_{D_l} c}{2 f_c}))^2}{2\sigma^2}} + eps.\end{aligned} \tag{21}$$

Here, t_r and t_v represent the range and velocity axes length, and eps is a small floating-point number to avoid nullity.

Algorithm 1 Proposed Target Estimation

Input: $\tilde{\boldsymbol{H}}$ - Estimated CFR
Output: $\boldsymbol{\delta_{(\hat{r}\hat{v})_l}}$ 2D-image

1) Build companion matrix $\boldsymbol{Q}$ as in (17);
2) Apply shift-inversion from (18) and calculate eigenvalues($\approx$ roots);
3) Extract roots $(\boldsymbol{v}(\boldsymbol{\psi})^H \boldsymbol{E_N} \boldsymbol{E_N}^H \boldsymbol{v}(\boldsymbol{\psi}) = 0\ ) < 1$;
4) Estimate $\hat{\tau}_\mathbf{l}, \hat{\mathbf{f}}_{\mathbf{D_l}}, \hat{\mathbf{r}}_\mathbf{l}$ and $\hat{\mathbf{v}}_\mathbf{l}$, from (12)-(15);
5) Minimize $||(\boldsymbol{I} - \boldsymbol{E_s}\boldsymbol{E_s}^T)\boldsymbol{v}(\boldsymbol{\psi})||^2$, $\forall(\hat{r}_l, \hat{v}_l)$ pairs;
6) Evaluate $\boldsymbol{\delta_{(\hat{r}\hat{v})_l}}$, from (20)-(23);

Note that the variance of the pulse allows flexibility in controlling the leakage of the sidelobes. Once the functions have been generated for each target, we could utilize the Kronecker product to get the 2D-root MUSIC estimates

$$\boldsymbol{\delta_{(\hat{r}\hat{v})_l}} = \boldsymbol{\delta_{\hat{r}_l}} \otimes \boldsymbol{\delta_{\hat{v}_l}}^T. \tag{22}$$

Here, T represents the transpose of the velocity pulse. For a range axis of length, $t_r = 0, 1, 2, ..., r_t - 1$ and a velocity axis of length $t_v = -v_t - 1, -v_t - 2, ..., 0, ..., v_t - 1$, where r_t being the arbitrary maximum range and v_t being the arbitrary maximum velocity, the above equation can be expanded as follows

$$\boldsymbol{\delta_{(\hat{r}\hat{v})_l}} = \begin{bmatrix} \delta_{\hat{r}_{l,0}} \cdot \boldsymbol{\delta_{\hat{v}_l}}^T \\ \delta_{\hat{r}_{l,1}} \cdot \boldsymbol{\delta_{\hat{v}_l}}^T \\ \vdots \\ \delta_{\hat{r}_{l,t-1}} \cdot \boldsymbol{\delta_{\hat{v}_l}}^T \end{bmatrix}. \tag{23}$$

The final 2D estimates can be further expanded and are given at the bottom of the page. The summarized target estimation framework is given in Algorithm 1.

V. Numerical Results

In this section, the numerical parameters, adapted from [13], and the simulation results for the proposed algorithm are discussed. For a 24 GHz radar with 4-QAM modulation, the number of subcarriers is taken as $N = 1024$ and the OCDM blocks are set to $M = 256$. To maintain the same overhead as [13], a total of $N_p = 32$ pilot blocks are used, evenly separated across M symbols. The signal bandwidth is $B = 113.92$ MHz with the subcarrier spacing to be 111.25 kHz making the symbol period $T = 8.988$ μsec. The length of cyclic prefix is set to $N/4$, which makes the total symbol period $T_0 = 11.236$ μsec. The variance of the Gaussian function is set to 0.1, while

$$\boldsymbol{\delta_{(\hat{r}\hat{v})_l}} = \begin{bmatrix} (e^{-\frac{(0-\hat{r}_l)^2}{2\sigma^2}}) \cdot (e^{-\frac{((-v_t-1)-\hat{v}_l)^2}{2\sigma^2}}) & \cdots & (e^{-\frac{(0-\hat{r}_l)^2}{2\sigma^2}}) \cdot (e^{-\frac{((v_t-1)-\hat{v}_l)^2}{2\sigma^2}}) \\ (e^{-\frac{(1-\hat{r}_l)^2}{2\sigma^2}}) \cdot (e^{-\frac{((-v_t-1)-\hat{v}_l)^2}{2\sigma^2}}) & \cdots & (e^{-\frac{(1-\hat{r}_l)^2}{2\sigma^2}}) \cdot (e^{-\frac{((v_t-1)-\hat{v}_l)^2}{2\sigma^2}}) \\ \vdots & \ddots & \vdots \\ (e^{-\frac{((r_t-1)-\hat{r}_l)^2}{2\sigma^2}}) \cdot (e^{-\frac{((-v_t-1)-\hat{v}_l)^2}{2\sigma^2}}) & \cdots & (e^{-\frac{((r_t-1)-\hat{r}_l)^2}{2\sigma^2}}) \cdot (e^{-\frac{((v_t-1)-\hat{v}_l)^2}{2\sigma^2}}) \end{bmatrix} \implies e^{-\frac{(t_r-\hat{r}_l)^2 + (t_v-\hat{v}_l)^2}{2\sigma^2}}, \forall(\hat{r}_l, \hat{v}_l)$$

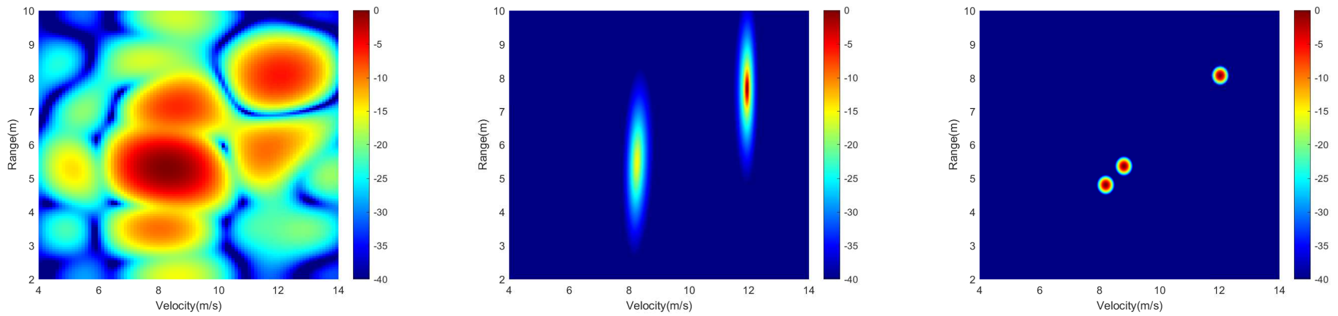

(a) (b) (c)

Fig. 2. Comparison of joint estimation of 2 correlated and 1 uncorrelated target using **(a)** 2D-FFT/Periodogram **(b)** 2D-MUSIC **(c)** 2D-root MUSIC (Proposed)

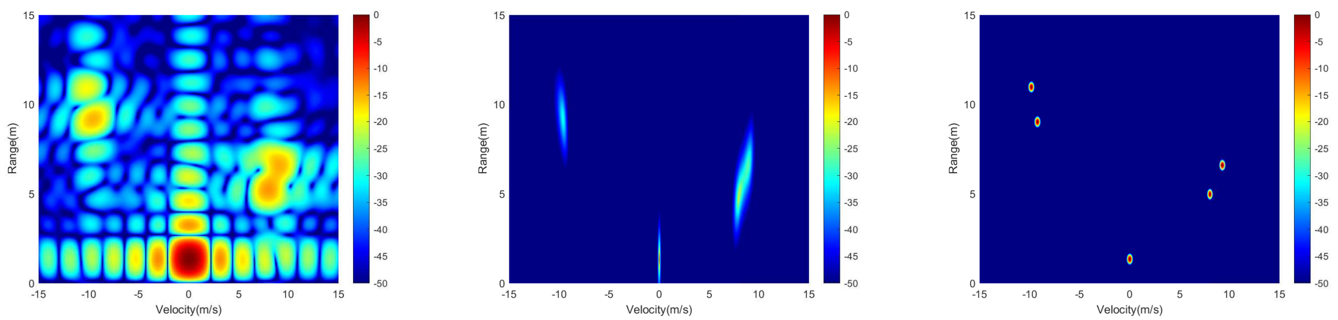

(a) **(b)** **(c)**

Fig. 3. Comparison of joint estimation of 5 highly correlated targets target using **(a)** 2D-FFT/Periodogram **(b)** 2D-MUSIC **(c)** 2D-root MUSIC (Proposed)

TABLE I
RADAR PARAMETERS

Sensing specification	Value
Maximum unambiguous range (R_{max})	1347 m
Range resolution (Δr)	1.3158 m
Maximum unambiguous velocity (V_{max})	555 m/s
Velocity resolution (Δv)	2.171 m/s

the smoothing factor is kept at 0.6 for 1D spatial smoothing, and the size of the sub-arrays for 2D spatial smoothing is $N_s = 12$ and $M_s = 12$. The radar specifications obtained for the mentioned parameters are listed in the Table I.

Two correlated signals, with ranges $r_1 = 5$ m and $r_2 = 5.8$ m and velocities $v_1 = 8$ m/s and $v_2 = 8.6$ m/s, in the presence of a third uncorrelated target at $r_3 = 7.5$ m and $v_3 = 12$ m/s, are considered at 0 dB SNR in Fig. (2), and compared with the traditional and proposed approach. 2D-FFT with huge sidelobes fails to detect the highly correlated pair and provides two approximate targets at $r_1 = 5.263$ m with $v_1 = 8.251$ m/s, and $r_2 = 8.092$ m with $v_2 = 12.159$ m/s. Although 2D-MUSIC sufficiently reduces the sidelobes, it does not distinguish the two correlated targets and provides $r_1 = 5.490$ m with $v_1 = 8.230$ m/s, and $r_2 = 7.652$ m with $v_2 = 11.921$ m/s. The proposed algorithm segregates two correlated targets at $r_1 = 4.796$ m with $v_1 = 8.186$ m/s, and $r_2 = 5.355$ m with $v_2 = 8.794$ m/s, both of which are within the tolerance of $\Delta r/2$ and $\Delta v/2$ from the actual ranges and velocities, and the third uncorrelated target at $r_3 = 8.065$ m with $v_3 = 12.018$ m/s.

In the second scenario in Fig. (3), 5 targets with two pairs of highly correlated targets and a stationary uncorrelated target is considered, at 5 dB SNR. The target ranges are at $r_1 = 1.3$ m, $r_2 = 5.6$ m, $r_3 = 6.5$ m, $r_4 = 9$ m, $r_5 = 10$ m, with velocities $v_1 = 0$ m/s, $v_2 = 8$ m/s, $v_3 = 9$ m/s, $v_4 = -9.3$ m/s, $v_5 = -10.3$ m/s. The first pair of highly correlated targets (2 and 3) are moving towards the radar, and the second correlated pair (4 and 5) is moving away from the radar, while target 1 is uncorrelated with any of the other correlated pairs. Due to the presence of sidelobes in typical 2D-FFT, the five targets are not easy to distinguish. Although three peaks are separable in the case of 2D-MUSIC Fig. 3(b), but due to the presence of sidelobes, the two correlated pairs cannot be separated. The leakage could be sufficiently reduced using the proposed method in Fig. 3(c), where Gaussian peaks are generated based on the peaks obtained by 1D root-MUSIC.

Performance evaluation in terms of root mean square error (RMSE) [13], [16] of velocity estimation for 2D-MUSIC and 2D-root MUSIC, is done for 2 cases in Fig. (4). The first case considers 2 highly correlated targets, while in the second case we consider 4 highly correlated targets, each separated with the randomly selected range and velocity difference. For correlated targets, random range difference is taken 0.8 m up to Δr, and random velocities with a difference of 1.3 m/s up to Δv are used. The range and velocities of each target

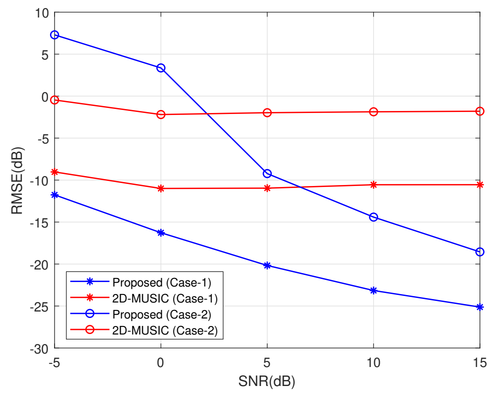

Fig. 4. RMSE of velocity for 2 highly correlated cases vs SNR

are also randomized from 0 m to 10 m, and 0 m/s to 10 m/s, respectively. As previously depicted in Fig. 2(b), due to leakage between pairs with high correlation, 2D-MUSIC does not distinguish the targets, while the proposed 2D-root MUSIC with improved sidelobes successfully detects correlated targets and thus provides a better RMSE as the SNR improves. However, given that the coefficients of the polynomial in the root algorithm become sensitive to perturbations in the presence of very large and strictly coherent targets (exactly the same range and velocity), if the available SNR is extremely low, such an improvement can be compromised and should be addressed in the future.

VI. Conclusion

In this study, a 2D-root MUSIC algorithm based on the OCDM RadCom system is proposed and compared with the conventional 2D-FFT and 2D-MUSIC approach to overcome spectral leakage issues, particularly in highly correlated targets. The simplified frequency domain OCDM sensing structure helps optimize computationally expensive conventional OCDM radars. The proposed method integrates a pulse-based algorithm for joint range and velocity estimation, utilizing an improved 1D-root MUSIC algorithm. Polynomial root reduction is performed to mitigate computational complexity while the correct assignment of multiple correlated targets is performed by minimizing the subspace residual error for all possible pairs. Simulation analysis for multiple highly correlated and uncorrelated targets indicates that the algorithm outperforms the computationally exhaustive 2D spectral search-based MUSIC, meanwhile the flexibility in controlling the sidelobes can be achieved by varying the variance of the Gaussian pulses. However, for a large number of strictly coherent targets or highly correlated targets in the same environment, such improved performance with reduced complexity requires a relatively higher SNR due to the inherent polynomial sensitivity of root MUSIC.

Acknowledgment

This work was supported in part by the Irish Research Council (IRC) under Grant GOIPD/2021/875 and Grant IRCLA/2022/3636, in part by Taighde Éireann – Research Ireland grant 12/RC/2276_P2_IPIC, and in part by the Enterprise Ireland (EI) under Grant CF-2021-1678-P.

References

[1] L. G. De Oliveira, B. Nuss, M. B. Alabd, A. Diewald, M. Pauli, and T. Zwick, "Joint radar-communication systems: Modulation schemes and system design," *IEEE Transactions on Microwave Theory and Techniques*, vol. 70, no. 3, pp. 1521–1551, 2021.

[2] F. Liu, C. Masouros, A. P. Petropulu, H. Griffiths, and L. Hanzo, "Joint radar and communication design: Applications, state-of-the-art, and the road ahead," *IEEE Transactions on Communications*, vol. 68, no. 6, pp. 3834–3862, 2020.

[3] C. Sturm and W. Wiesbeck, "Waveform design and signal processing aspects for fusion of wireless communications and radar sensing," *Proceedings of the IEEE*, vol. 99, no. 7, pp. 1236–1259, 2011.

[4] H. S. Rou *et al.*, "From Orthogonal Time–Frequency Space to Affine Frequency-Division Multiplexing: A comparative study of next-generation waveforms for integrated sensing and communications in doubly dispersive channels," *IEEE Signal Processing Magazine*, vol. 41, no. 5, pp. 71–86, 2024.

[5] P. Raviteja, K. T. Phan, Y. Hong, and E. Viterbo, "Orthogonal Time Frequency Space (OTFS) modulation based radar system," in *2019 IEEE Radar Conference (RadarConf)*, pp. 1–6, 2019.

[6] Y. Ni, Z. Wang, P. Yuan, and Q. Huang, "An AFDM-based integrated sensing and communications," in *2022 International Symposium on Wireless Communication Systems (ISWCS)*, pp. 1–6, 2022.

[7] L. G. De Oliveira, M. B. Alabd, B. Nuss, and T. Zwick, "An OCDM radar-communication system," in *2020 14th European Conference on Antennas and Propagation (EuCAP)*, pp. 1–5, IEEE, 2020.

[8] X. Ouyang and J. Zhao, "Orthogonal Chirp Division Multiplexing," *IEEE Transactions on Communications*, vol. 64, no. 9, pp. 3946–3957, 2016.

[9] S. Bhattacharjee, K. V. Mishra, R. Annavajjala, and C. R. Murthy, "Evaluation of Orthogonal Chirp Division Multiplexing for automotive integrated sensing and communications," in *International Conference on Acoustics, Speech and Signal Processing*, pp. 8742–8746, IEEE, 2022.

[10] S. Bhattacharjee, K. V. Mishra, R. Annavajjala, and C. R. Murthy, "Multi-carrier wideband OCDM-based THz automotive radar," in *International Conference on Acoustics, Speech and Signal Processing (ICASSP)*, pp. 1–5, IEEE, 2023.

[11] R. Schmidt, "Multiple emitter location and signal parameter estimation," *IEEE transactions on antennas and propagation*, vol. 34, no. 3, pp. 276–280, 1986.

[12] R. Roy and T. Kailath, "ESPRIT-estimation of signal parameters via rotational invariance techniques," *IEEE Transactions on acoustics, speech, and signal processing*, vol. 37, no. 7, pp. 984–995, 1989.

[13] J. B. Sanson, P. M. Tomé, D. Castanheira, A. Gameiro, and P. P. Monteiro, "High-resolution delay-doppler estimation using received communication signals for OFDM radar-communication system," *IEEE Transactions on Vehicular Technology*, vol. 69, no. 11, pp. 13112–13123, 2020.

[14] X. Ouyang, O. A. Dobre, Y. L. Guan, and P. Townsend, "Channel estimation for Multiple-Input Multiple-Output Orthogonal Chirp-Division Multiplexing systems," *IEEE Transactions on Wireless Communications*, vol. 23, no. 1, pp. 436–449, 2024.

[15] X. Ouyang, C. Antony, F. Gunning, H. Zhang, and Y. L. Guan, "Discrete fresnel transform and its circular convolution," *arXiv preprint arXiv:1510.00574*, 2015.

[16] R. Xie, D. Hu, K. Luo, and T. Jiang, "Performance analysis of joint range-velocity estimator with 2D-MUSIC in OFDM radar," *IEEE Transactions on Signal Processing*, vol. 69, pp. 4787–4800, 2021.

[17] M. Henninger, S. Mandelli, M. Arnold, and S. Ten Brink, "A computationally efficient 2D MUSIC approach for 5G and 6G sensing networks," in *2022 IEEE Wireless Communications and Networking Conference (WCNC)*, pp. 210–215, IEEE, 2022.

[18] G. W. Stewart, "A Krylov–Schur algorithm for large eigenproblems," *SIAM Journal on Matrix Analysis and Applications*, vol. 23, no. 3, pp. 601–614, 2002.

[19] X.-Y. Zhang, J. Zhang, Y.-J. Gong, Z.-H. Zhan, W.-N. Chen, and Y. Li, "Kuhn–Munkres parallel genetic algorithm for the set cover problem and its application to large-scale wireless sensor networks," *IEEE Transactions on Evolutionary Computation*, vol. 20, no. 5, pp. 695–710, 2015.